

THE ROYAL INSTITUTION OF NAVAL ARCHITECTS

ON THE ROLL DAMPING OF AN FPSO WITH RISER BALCONY AND BILGE KEELS

R van 't Veer, SBM GustoMSC, The Netherlands

F Fathi, SBM GustoMSC, The Netherlands

SUMMARY

Although the topic of roll damping of vessels at sea is already brought to the attention of naval architects by Froude more than 100 years ago, the physics of it remain intriguing, even today. An accurate prediction of the motions of offshore structures in harsh environments, designed for 25 years continuous operation, is the topic of this paper. Model test experiments for two FPSO's developed by SBM for Petrobras are discussed. It is shown that the FPSO submerged riser balcony on one side of the vessel contributes to the roll damping through similar physics as the bilge keel does. Flow memory effects are discussed in detail since these are shown to have a noticeable effect on the roll damping coefficients. The paper further employs 3D CFD simulations to enhance the understanding of the fluid behaviour around the FPSO appendages, necessary to construct a rational and accurate roll damping model in the future.

1. INTRODUCTION

This paper addresses the motion behaviour of a Floating Production Storage Offloading (FPSO) unit intended to operate offshore Brazil in deep water conditions. The FPSO is a converted VLCC tanker that will be spread-moored at location. It is designed for 25 years continuous offshore operation. The FPSO will receive the crude oil produced from subsea wells via a large number of risers. These risers connect to a submerged lower riser balcony and then run vertically along the hull side to the upper riser balcony located just below the main deck level. An artist impression of the FPSO is given in Figure 1 showing the risers on port side, mid ship.

The roll motion behaviour of an FPSO with riser balcony and bilge keels was first studied, in 2008, through model tests for the P-57 FPSO (denoted FPSO-1 in this paper). The model tests were conducted at MARINTEK at scale 1:60. This FPSO is due to start oil production at the end of 2010. A recent picture of the FPSO is seen in Figure 2. For another project SBM is involved in for Petrobras, a similar VLCC hull as the P-57 is being converted to the Cidade de Paraty FPSO (denoted FPSO-2 in this paper). This FPSO is to commence oil production in 2013. Due to the significant larger riser balcony on FPSO-2, sea keeping model tests at scale 1:60 were performed for this FPSO at OCEANIDE basin mid 2010. Experiences from the two model test series related to roll damping are presented in this paper.

Over the last years, SBM is strengthening their Computational Fluid Dynamics (CFD) group and making significant progress in applying CFD simulations in various projects. In view of this, roll decay simulations with FPSO-1 were undertaken to verify and validate application of CFD for the estimation of roll damping of complex geometries like this FPSO with a riser balcony and truncated bilge keel on one side of the vessel and a full length bilge keel on the opposite side. Insights from these CFD simulations are presented in this paper.



Figure 1: Artist impression of the Cidade de Paraty FPSO



Figure 2: P-57 FPSO

2. VESSEL GLOBAL MOTION ANALYSIS

2.1 INTRODUCTION

Continuous operation through 25 years lifetime implies that the global vessel motions, even in extreme sea states, should be limited. For a spread-moored vessel, this is to

be verified early in the design stage for all design extreme conditions; the DEC sea states. The DEC sea states are defined as those Hs-Tp combinations that have 100-year return period. The bilge keel dimensions are selected such that the vessel complies with the requirement that the most probable maximum roll amplitude does not exceed 10 degrees in any DEC sea state.

2.2 MOTION EQUATIONS

The damping from the bilge keel and riser balcony is associated with vortex separation at the sharp corners of the appendages (viscous damping). This non-linear roll damping is accounted for by an added quadratic damping coefficient in the global motion equations, which are based on non-viscous potential flow hydrodynamics. The coupled 6DOF motion equations are then iteratively solved in each sea state using stochastic linearization [1] [2]. This result in sea state dependent motion response spectra in which the proper equivalent linear damping is utilized. Model test for the FPSO-1 showed that the catenary mooring damping can be represented through a quadratic roll damping coefficient as well. The non-linear damping from the catenary mooring lines (and risers) is associated with a Morison type of drag damping.

From the motion spectra the most probable maximum motion amplitudes are calculated based on the number of wave cycles in the irregular 3 hour sea state. It is thereby assumed that the amplitude distribution obeys a Rayleigh distribution. For a non-linear motions as roll this is not necessarily the case. In fact, it would be more precise to fit a (Weibull) distribution to the measured motion amplitudes in the model tests and to use this distribution (and its coefficients) to calculate the most probable extreme. However, it is questionable if a distribution fit to a non-linear response in a particular (long crested) sea state at a particular vessel heading is generally valid for that DOF at all other headings and in all other sea states; most likely it is not. This issue is not further discussed in this paper. The approach taken is to assume that the Rayleigh distribution can be used to predict the most probable maximum amplitude for all DOF's, including roll, based on the motion zero spectral moment.

The (iterative) stochastic linearization technique with a quadratic roll damping coefficients can be easily and generally applied in engineering studies [2] [3]. The quadratic coefficient is then linearized through an equivalent velocity, or the standard deviation of the velocity spectrum in an irregular sea state. An assumption often made is that the quadratic damping coefficient is valid for a given loading condition of the vessel and that it can be applied in all sea states, low and high and with peak period near or further away from the natural period. It means that the damping coefficient (or drag coefficient) is considered to be independent of the motion amplitude. This is generally not the case since the

drag coefficient of an oscillating plate (appendage) varies with the oscillation character expressed by the Keulegan-Carpenter number (KC) [4].

The vessel hydrodynamics are calculated through linear 3D potential flow calculations in the frequency domain. In such calculations only the hull wetted surface below the calm waterline is utilized. Calculations have shown that the riser balcony is to be included in the hull mesh to obtain correct global vessel hydrodynamic coefficients. Linear radiation and diffraction coefficients and linear restoring are considered valid in all sea states. The adaption, or calibration of the motion equations is only done through the non-linear roll damping coefficient. Due to the riser balcony, the vessel response is asymmetric with respect to waves coming from port side or starboard side.

2.3 NON-LINEAR DAMPING

A convenient method to measure the system damping is through an extinction test. The system is brought to imbalance by an external moment. After release the system decays to the equilibrium condition. When the damping is far below the critical damping, the transient decay is oscillatory. A methodology to analyse the decay is the logarithmic decrement method, as presented in many references, like [4] [5] [6]. Different parametric models can be used, but overall the linear-plus-quadratic damping model gives a good fit to experimental data in naval application [6] [8].

The two extinction coefficients derived from it, denoted a and b in [6], are directly related to a linear damping coefficient B1, and a non-linear damping coefficient B2, respectively, see section 5.1. It is common practise to derive a single B2 coefficient through a least-square fit on the data points in the extinction test analysis. This means that the amplitude or KC dependency of the non-linear damping is lost. The linear damping B1 found in a decay ideally matches with the linear damping as calculated by potential flow.

In the motion analysis for the two FPSO's, a sea state and heading independent B2 damping coefficient was adopted, but this value was calibrated such that the motion spectra through stochastic linearization matched the measured spectra in the model basin. This requires model tests in irregular seas with wave spectra valid for the location where the FPSO will operate. Since the objective is to obtain an accurate motion prediction in extreme sea states, the calibration to wave spectra is considered more relevant and accurate than to use a damping measured in the decay tests in calm water. For these FPSO's, the damping in waves was found to be higher than the damping in the free-decay in calm water.

However, in this paper our main focus is to report on the roll decay tests. Such tests were performed in the model basin and through CFD simulations. Both the model tests and CFD results show important physical

phenomena and thereby increase insight in how non-linear roll damping can be accounted for in a sea state. It is clear that 6DOF CFD simulation of a vessel in a 3 hour duration sea state is far beyond current practice and such is not expected to be feasible in the near future. But a CFD roll decay test in calm water with a 3D appended model is feasible and requires typically about 2 week computing time on a 12 cores cluster.

This paper investigates to sensitivity and accuracy of the damping coefficients as derived through free-decay extinction experiments carried out in the towing tank and in CFD simulations. The sensitivity of the non-linear damping in the motion prediction is given in Section 7.

3. FPSO VESSEL PROPERTIES

The two FPSO's addressed in this paper are converted sister-ship VLCC tankers. The typical dimensions are 320 m in length and 56 m in beam. The draught will vary between approximately 7 m in ballast loading condition and 20 m in loaded condition. The KG of FPSO-2 is 18.2 m in ballast and 15.2 m in loaded condition, which leads to a GMT of 18.2 and 7.7 m, respectively. The loading condition properties for FPSO-1 are comparable to this.



Figure 3: Lower and upper riser balcony on FPSO-1 (top) and FPSO-2 (bottom).

The dimensions of the lower riser balcony are about 77 m in length by 4.7 m in width for FPSO-1, and 105 m by 5 m for FPSO-2. The layout of the balcony is quite different between the two FPSO's, as can be seen on the model test photos in Figure 3. On FPSO-1 the riser balcony layout is box shaped, on FPSO-2 a staggered

layout is used. The representation of the balcony at model scale is somewhat simplified compared to the real design, for the ease of model fabrication, and based on the hypothesis that not all small details will influence the damping. The risers running between the lower and upper balcony are considered to have minor influence on the damping and were left out on the FPSO-2 model.

To avoid possible riser damage there is no bilge keel below the riser balcony. The final bilge keel height was set to 1.2 m for both vessels.

Model tests with FPSO-1 (and mooring line calculations) showed that the influence of the catenary mooring on the roll damping is significant and must be accounted for in a motion prediction. But, in all results presented in this paper the catenary mooring is excluded.

4. COMPUTATIONAL FLUID DYNAMICS

4.1 NUMERICAL METHOD

The CFD time domain simulations presented in this paper are obtained with StarCCM+. The time dependent incompressible Navier-Stokes equations are solved in their statistical Reynolds averaged (URANS) formulation. StarCCM+ uses a finite volume discretization on a collocated grid (Rhie and Chow interpolation) to determine the time evolution of the flow field. For all the equations, a second order discretization scheme is used for the advection terms. The presence of both air and water is modelled by the volume of fluid (VOF) method. The free-surface is defined as the iso-surface of cells with 50% water/air contents. Both air and water are modelled as incompressible fluids. Momentum and continuity equations are coupled through a variant of the SIMPLE algorithm and the solvers are accelerated using a Multigrid algorithm.

The URANS formulation implies a closure modelling of the averaged cross products of the fluctuating terms which are solved by the classical 2-equation eddy viscosity model known as Menter's Shear Stress Transport (SST) model [10]. Following Boussinesq's assumption, the Reynolds stresses are considered proportional to the fluid shear stresses. The turbulent viscosity is an anisotropic model for the added energy dissipation, occurring in the fluid because of turbulence. Its effect is taken into account by adding it to the fluid viscosity.

To calculate the free floating body motion, an iterative coupling is used between the CFD solver and a rigid body solver. In order to accommodate for the hull motions, the mesh has to be modified at each time step. The mesh transformation strategy is discussed in the next section. Time integration of the flow equations is carried out through a 1st order implicit scheme. The time step is defined as 1/100 of the estimated roll period.

4.2 COMPUTATIONAL SETUP

The geometry used to represent the FPSO in the simulation is a 3D CAD model of the hull including the bilge keels, rudder and lower riser balcony. The risers are not included and the balcony is simplified into a rectangular block. For meshing purpose the bilge keels have additional thickness.

The 3D computational mesh has been generated using the trimmed mesher of StarCCM+. It mainly consists of hexahedrons aligned with the still water free surface plane. Refinement is carried out by cell subdivision with hanging nodes. The mesh is refined around the free surface and the hull with additional refinement around the bilge keels and the submerged riser balcony. To properly account for wall turbulence, a prism layer mesh is extruded from the quadrangle surface mesh at the hull. The prism layer features 15 divisions with a moderate expansion factor of 1.2. This leads to a total mesh size of about 2.7M cells. Away from the hull, the grid cells are coarsened in the wave propagation direction in order to generate numerical damping of the radiated waves and avoid wave reflection at the boundaries. By coupling this meshing technique with a long domain span of 15*B, boundary effects on the simulation can be neglected.

In order to accommodate the roll motion, the mesh is divide into two domains that allows the hull to rotate using embedded mesh motion, see Figure 4. The internal domain is cylindrical and includes the hull surface and the mesh around the hull. It rotates rigidly following the motions of the vessel. The external domain, delimited by the outer surface of the inner domain cylinder and the external boundaries, is not allowed to rotate. To ensure continuity, the flow variables are interpolated from each side of the cylinder at the sliding interface. This method is robust as compared to mesh deformation or remeshing techniques, with as drawback that it takes significant computational time in the interpolation process.

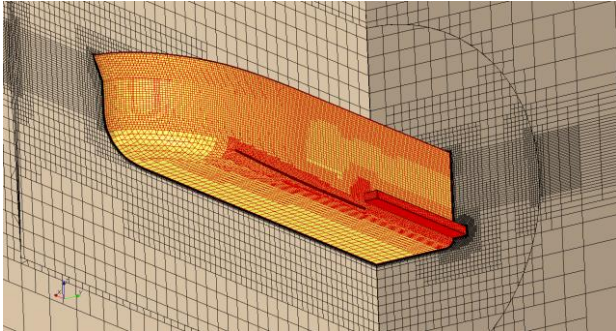


Figure 4: Part of the 3D CFD mesh with the bilge keel and riser balcony

In a single degree-of-freedom (SDOF) simulation, the internal mesh (with the FPSO) rotates around the prescribed centre of rotation set in the water plane. Due to the riser balcony volume, the centre of buoyancy in equilibrium floating condition is slightly off from the

centreline and the centre of rotation is shifted accordingly. The body motions are solved with respect to this origin. The mass inertia, as defined with respect to the centre of gravity of the FPSO, is set at the centre of rotation without modification. All simulations start with a flow at rest (flat free surface and hydrostatic pressure).

5. ROLL DECAY TESTS

5.1 LOGARITHMIC DECREMENT METHOD

The logarithmic decrement method is used to determine the linear (B1) and quadratic (B2) roll damping coefficients. The roll motion equation is thereby decoupled from the other motion modes, thus a single degree-of-freedom analysis is applied. The general SDOF motion equation for free decay is given by:

$$M\ddot{x} + B_1\dot{x} + B_2\dot{x}/\dot{x} + Cx = 0$$

where M represents the structural and added mass, and C the system restoring. When this equation is linearized it reads as:

$$\ddot{x} + 2\zeta_E\omega_0\dot{x} + \omega_0^2x = 0$$

where ω_0 is the natural frequency of the system in air with $\omega_0 = \sqrt{C/M}$, and ζ_E stands for the equivalent linear damping, which can be written as:

$$\zeta_E(x) = \frac{\gamma}{\omega_0} = \frac{B_E}{B_{crit}} = \frac{B_1}{B_{crit}} + \frac{B_2}{B_{crit}} \frac{16}{3T_d} x$$

with the critical damping $B_{crit} = 2\sqrt{CM}$, and T_d as the damped oscillation period. The term $(16/3T_d)x$ is an equivalent velocity. The damped and undamped oscillation frequency relate to each other by $\omega_d = \sqrt{\omega_0^2 - \gamma^2}$. With this notation the logarithmic decrement is the ratio between two consecutive amplitudes, and when these are one period apart, the decrement for the j -th oscillation is given by:

$$\delta_j = \ln\left(\frac{x_j}{x_{j+T_d}}\right) = \gamma_j T_d = \frac{2\pi\zeta_j}{\sqrt{1-\zeta_j^2}}$$

The damping coefficients are derived from the coefficients a and b that fit the decrement data points in a least-square sense:

$$B_1 = \frac{a}{\pi} \frac{C}{\omega_n} = 2a \frac{I + A(\omega_n)}{T_n}$$

$$B_2 = \frac{3}{8} b \frac{C}{\omega_n^2} = \frac{3}{8} b \frac{I + A(\omega_n)}{\omega_n^2}$$

where I is the mass inertia and $A(\omega_n)$ is the added mass at the (damped) natural frequency, C is the restoring term. The coefficient a is the value at zero amplitude, b is the slope of the trendline, see Figure 5.

As pointed out by Himeno [6], only the amplitude independent part of the non-linear damping is related to the b coefficient. The part that is proportional to the amplitude will appear in a cubic damping term (not included in the above equations) and the part inversely proportional to the amplitude is transferred to the linear damping coefficient a .

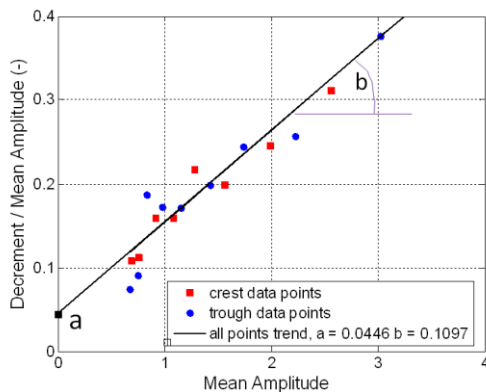


Figure 5: Example of decay decrement analysis

5.2 FLOW MEMORY EFFECTS

In Figure 6 two time traces of a model test roll decay are shown. One test shows a decay in which the model is slowly brought to a roll angle before the decay starts. This is denoted as a held-over decay test. In the other test the vessel was brought to larger angles through a number of oscillations before the free-decay starts. This is denoted as a decay method with pre-oscillations.

In the held-over decay the vessel is brought to about -14 deg. The riser balcony then moves up in the first half decay period. In the decay with pre-oscillations the vessel is four times excited with a positive roll moment (balcony moving up). The motion to the opposite roll angle is not a forced motion. The start of the decay analyses is therefore at the amplitude peaks indicated by the markers in Figure 6.

The damping decrement result is presented in Figure 7. The held-over decay clearly shows that the damping decrement between the first two troughs (ref t1-t2) and the first two crests (ref c1-c2) is much lower than the damping decay rate in the following oscillations. This is considered to be a memory effect related to the fact that in the held-over decay the fluid starts from rest without any disturbances near the vessel. Although the difference is less significant, the third oscillation period decrement in the held-over decay shows less damping than for this oscillation period (amplitude level) in the transient decay

with pre-oscillations, while the fourth decrement point shows a larger damping rate in the held-over test. In successive oscillations the damping is very similar.

From the decay analysis, no different damping rate or behaviour is observed between the situation that the balcony moves upwards or downwards.

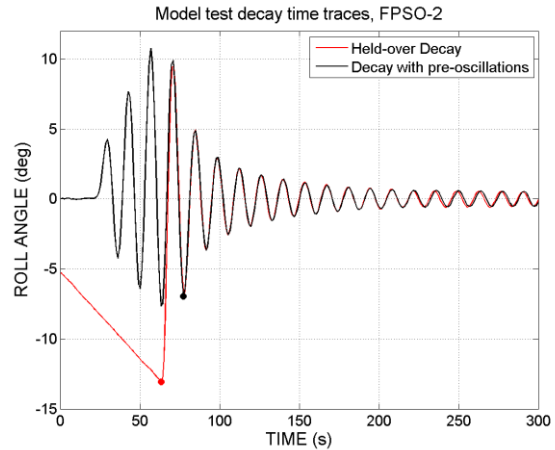


Figure 6: Model test roll decay time traces

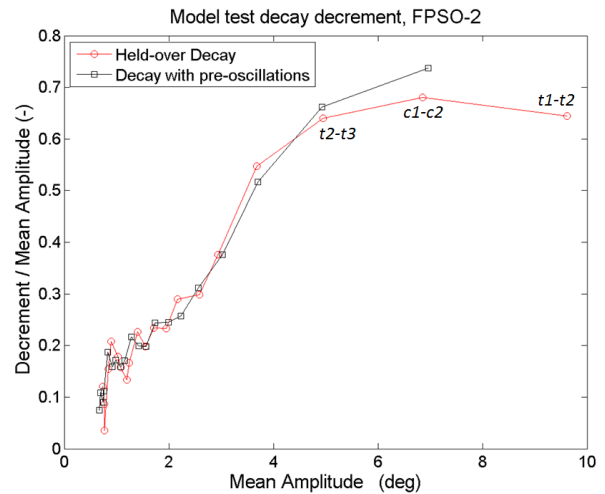


Figure 7: Model test roll decay decrement plot

The influence of initial fluid disturbances on the damping decay was investigated as well in CFD simulations. In Figure 8 two time traces of a SDOF roll decay simulation are shown. In the held-over simulation the initial flow field is completely at rest at the start of the decay. Only for clear comparison with the other simulation, the time trace is shifted so that the free-decay starts at the same time in the plot. In this simulation the flow field is at rest at $t=0$ s. The two time traces show distinct differences in the first two oscillations, and compare well afterwards. This results in a very different damping decrement, as can be seen in Figure 9, even for the smaller amplitude oscillations. The decay rate with pre-oscillations shows a rather constant slope which means that it can be well

represented with a single B2 value. Without pre-oscillations the damping decay is much lower in the first oscillation, and then overshoots the trendline. This is comparable to the findings in the model test experiments. The fact that the memory effects are much stronger in CFD than in the comparable (but not identical) model tests might be due to the fact an initially completely undisturbed flow is unlikely in the model test basin. Based on these finding, it is concluded that a decay model test or CFD simulation without any initial flow disturbances can lead to inaccurate or unrealistic damping values, since there is always a history to vessel motions.

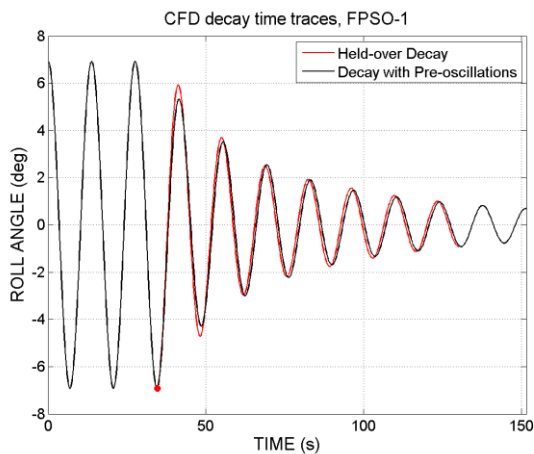


Figure 8: CFD roll decay time traces

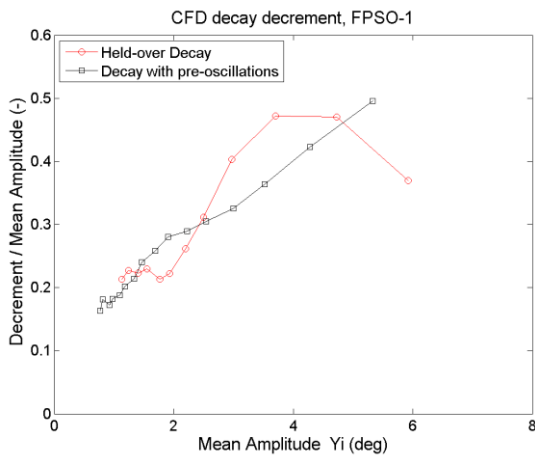


Figure 9: CFD roll decay decrement plot

The importance of flow memory effects in roll damping is already discussed by Ikeda et al [7]. In a Morison equation the instantaneous velocity and acceleration are used, and there is thus no flow memory accounted for. The same is seen in the logarithmic decrement method where an equation without memory is fitted to the decay. Ikeda [7] shows through experiments that the drag coefficient on plates increases in the first few oscillations when started with a flow in rest. It takes about 3 to 4

oscillations before a steady-state flow field is established and the drag becomes constant. For all KC numbers investigated (defined as $KC = UT / 2h$, where U is the maximum flow velocity in the oscillation period T , and h as bilge keel height) the drag coefficient in the first oscillation is about half the value found in steady condition. The effect is contributed to the interaction between old and new vortices. Only after a few oscillations a kind of steady disturbed flow field exist around the object. A further valuable observation reported from the experiments by Ikeda [7] is that the memory effects remain important in irregular motion. When the previous oscillation has a larger amplitude the drag coefficient is larger than at steady oscillation amplitude. When the previous oscillation is smaller in amplitude the drag coefficient is similar to the drag found in the first oscillation starting from rest.

The findings from the free-decay basin experiments and CFD simulations support the observations from Ikeda [7]. The absence of flow vortices in a held-over decay will decrease the damping in the first oscillation period. The successive oscillations might then suffer from a too large damping 'coefficient' since the amplitudes in successive oscillation are smaller than the previous oscillation. It might be true that the damping decrement 'stabilizes' after a few oscillations due to the fact that the fluid is fully disturbed, although this remains uncertain. It raises interest in the velocity field, and related memory effects, the vessel will experience in a sea state when orbital velocities transport the previous generated vortices away or perhaps towards the vessel. In a sea state, the most probable amplitude is always preceded by smaller amplitudes and the findings suggest that the roll damping might than be smaller than an equivalent damping derived from a decay test or forced oscillation test carried out at that amplitude. A forced oscillation test at the most probable amplitude is thus also not a proper method to find the equivalent damping for the most probable roll amplitude in a sea state.

5.3 THE ACCURACY OF A DECAY ANALYSIS

Since the maximum roll amplitudes of the FPSO should not exceed 10 degrees, it implies that in a DEC sea state the significant roll amplitude is about 6 degrees. We are thus concerned with an accurate damping prediction at relative small angles.

As demonstrated in Figure 7 and Figure 9, the vessel decay damping cannot be exactly described by a linear and quadratic damping, although to large (and practical) extent it can. The trendline slope representing B2 is found using a least square fit on all data points. This means that the decay rate at small and large amplitudes is accounted for with the same weight. The scatter often seen in the data points at small amplitude are thus of concern since they influence the B2 as much as the few data points found at larger roll amplitude.

The accuracy of the decay tests and the relevance of the mathematical damping model (linear, quadratic, cubic) are discussed by many researchers (e.g. [4], [8] [9]). The quadratic damping model prevails as the most representative, although it is often discussed that such a model does not captures the (possible) important KC dependency of viscous flow separation through the drag coefficient.

The scatter in the logarithmic decrement method at small amplitudes should in modern test facilities not originate from inaccurate measuring equipment, data noise or data drift. And it is our experience that the scatter at low amplitudes can be found in model test data from many vessels tested in different model basins. Possible causes could be: coupling between the translation and rotation modes, remaining basin turbulence due to previous oscillations or experiments, wave reflections from tank walls or beaches and, most likely with a significant contribution, the stochastic nature of vortex separation at sharp edges leading to flow memory effects. Even if the time traces show marginal differences, it can lead to significant different damping ratios. This can be seen not only when using the decrement method, but as well when a fit is made to the time trace curve. Obviously, because both approaches are similar. Data filtering might decrease the scatter but it is a sensitive approach and it is often difficult not to influence the larger amplitudes of the decay. To decrease the influence of data scatter, the quadratic damping coefficient can be derived from data points that are most relevant for the final motion prediction. This requires proper decay test parameters and procedures.

In Figure 10 the time traces are shown from four decay experiments with FPSO-1 which only differ in the starting angle of free-decay. All decays were preceded by several oscillations. The decrement plot is given in Figure 11 and it exhibits a large variation in B2 coefficients derived by fitting the data points to a linear trendline. It is clear that a few data points can influence a fit considerably, giving different linear (B1) and quadratic (B2) damping values. In this model test example, the quadratic damping coefficients obtained increase when the decay starts from a larger amplitude, while the linear damping coefficients decreases. The variation is large: B2 increases by 30.1% from decay test04 to decay test03, and B1 decreases by 29.8%. Given a certain amplitude level, the absolute damping is than very similar, e.g. at 2 deg, or not so similar. For example at 4 deg the equivalent damping differs by 10.3%.

A second attempt to derive a unique B2 from the four different decay tests used before is given in Figure 12. In this analysis all amplitudes below 1.0 deg are skipped. Now the B1 and B2 coefficients are rather similar, which is however merely related to the selected truncation value than to the physics. Using a truncation of for example 0.8 deg leads to very different coefficients. A further

comparison shows that the B2 coefficients from decay04 in Figure 12 (using limited data points) is 6.1% lower than the B2 coefficient obtained in Figure 11.

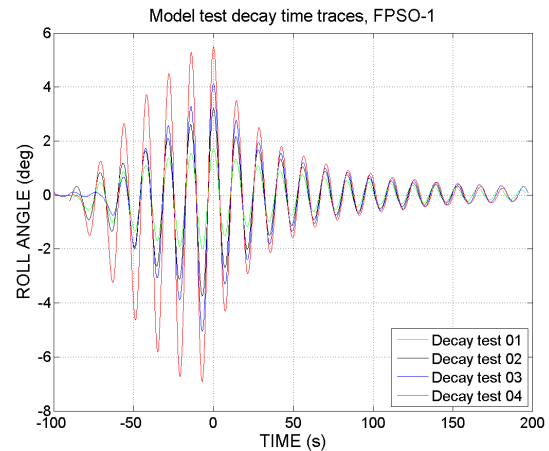


Figure 10: Model test decay time trace comparison

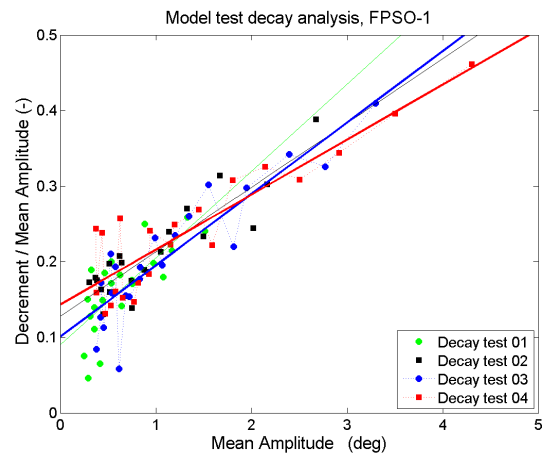


Figure 11: Model test decay analysis comparison

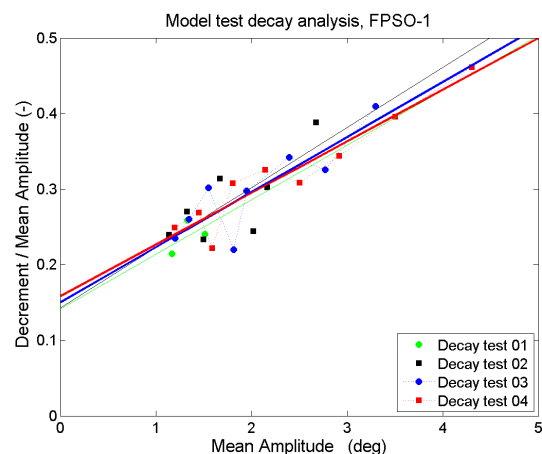


Figure 12: Model test decay analysis using only roll amplitude above 1.0 deg

The influence of the starting angle of the decay has been investigated through SDOF CFD simulations on FPSO-1. The loading condition in CFD is the same as in the basin experiments, but in CFD the rotation point is set in the water plane as discussed earlier. The two CFD decay simulations only differ in the initial roll angle: one start at 6.92 deg, the other at 5.75 deg. Before the model is set free to decay, $2\frac{1}{2}$ period of pre-oscillations with constant amplitude are imposed. The decay starts, as in the model tests, with the balcony at its lowest point (negative roll angle). The time traces are seen in Figure 13, the decay analysis plot is given in Figure 14.

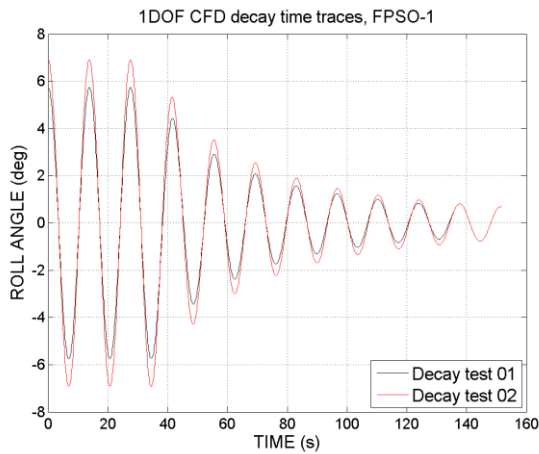


Figure 13: CFD decay time trace comparison

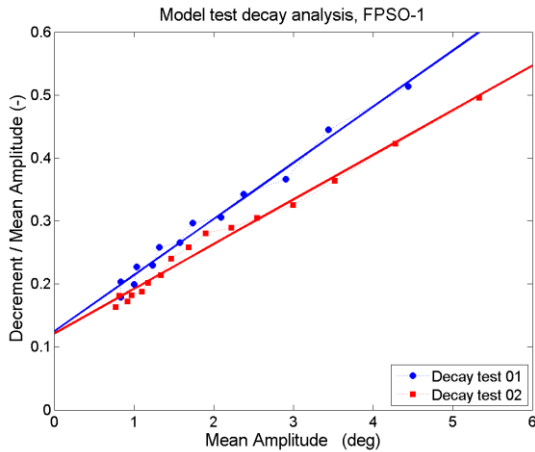


Figure 14: CFD decay analysis comparison

In the CFD results the scatter at low amplitudes is less significant than in the model tests, with the remark that the CFD simulations end much earlier and does not include very small amplitudes (7 oscillations in CFD versus 12 oscillations in model tests). Less data scatter at low amplitude is favourable to obtain a unique linear damping, and between the two simulations the difference in B_1 is only 2.8%. The quadratic damping is however very different. The quadratic damping in the decay from 5.75 deg is 25.6% larger than in the decay from 6.92 deg. This difference in quadratic damping is comparable to

the findings in the model tests, and it shows the same trend: starting the decay at lower amplitudes can lead to a larger quadratic damping.

Comparing model tests and CFD shows that for this FPSO case the quadratic damping from CFD (test02) is 2.3% lower than the quadratic damping in the model test (test04). The linear damping coefficient is 15.2% lower in CFD than in the model test. The simulation result compares thus very well with the experimental result, which is encouraging for future application.

The discussion in this section highlights that, although in theory a free decay seems the most simple and practical method to establish the amount of quadratic roll damping, there are many physical issues related to it. To a large extend these are related to flow memory contributions. The capability to perform in CFD a 3D roll decay simulation with a complex vessel in SDOF is shown. Further CFD studies, like mesh convergence and application to other vessels, are to be carried out to confirm application. However, proper validation of CFD with model basin data remains problematic and most likely requires an exact replay of the model test experiment to match the fluid history between both as to avoid flow memory effects or incorrect conclusions on the accuracy of the CFD simulations.

6. CFD FLOW OBSERVATIONS

CFD allows us, when the simulation is done, to study the flow behaviour around the appendices without any additional simulation cost. The only problematic issue is that flow visualisation requires such huge amount of data storage that it is practically impossible to save the data from each time step. The flow observations are therefore limited to a few events.

In Figure 15 and Figure 16, the velocity field (mid ship plane) for both the held-over and the pre-oscillated test are shown. The snapshot corresponds to $t=\frac{1}{4}T$, which is the first even keel position in the decay, also corresponding to the maximum global roll velocity. At this moment the balcony is moving upwards in the first free-decay oscillation. The flow field near the balcony and the bilge keel are shown. In spite of the obvious geometric differences, the behaviour of the flow around the bilge keels and the balcony exhibit important similarities. The two type of appendages will therefore be discussed together. Note that the velocities in the figures are model scale (1:60) values, since CFD simulations were performed at this scale.

The flow detachment at a sharp edge results in a large vortex. It is associated with a low pressure on the downstream side of the balcony or the bilge keel. The size of the vortex is related to the fluid velocities upstream of the appendage and these are directly related

to the over pressure on this side of the appendage. The size and intensity of the detached vortex are therefore a good qualitative indicators of the amount of roll damping induced by the appendages.

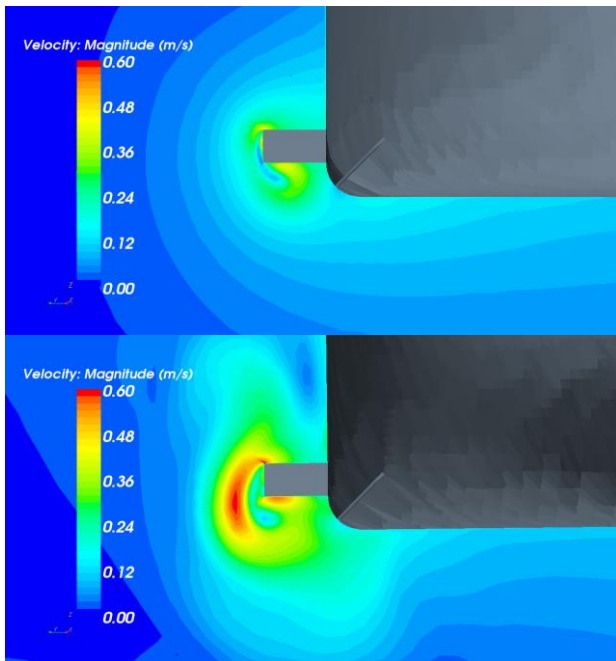


Figure 15: Velocity field around the balcony at $t=1/4T$. Top: Held-over decay, bottom: Decay with pre-oscillations

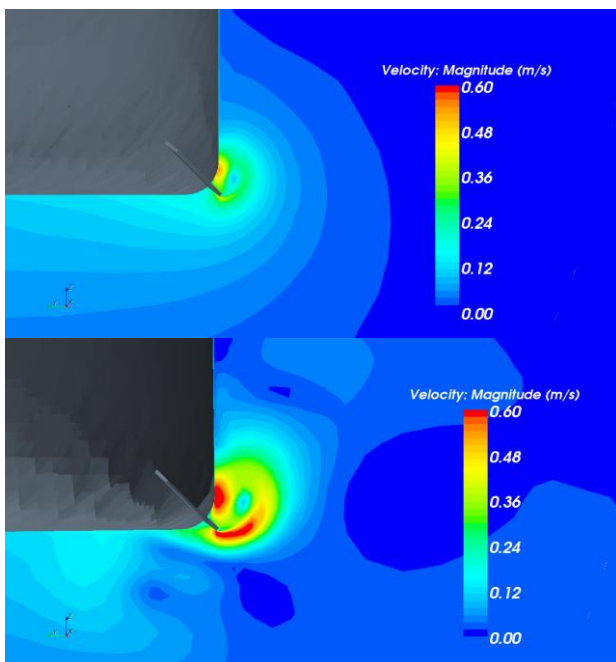


Figure 16: Velocity field around the bilge keel at $t=1/4T$. Top: Held-over decay, bottom: Decay with pre-oscillations

A distinct different velocity field is seen between the held-over decay (top) and the decay with pre-oscillations (bottom). After $1/4$ of decay period, more turbulence is observed in the flow with pre-oscillations than in the held-over situation. This is true around the appendage

flow detachment point as well as in the vicinity of the hull surface.

In Figure 17 the velocity field is seen at the start of the free-decay for the CFD simulation with pre-oscillations. Instead of a zero fluid velocity field, as it would be in the held-over decay, a distinct ‘developed’ flow field is observed. This flow field is responsible for the flow memory effects at this time event. While the vessel has reached its maximum roll angle, the fluid, due to its inertia, is still flowing around the hull. It creates a flow detachment around the bilge keel tip and interferes with the vortex created by the bilge keel. This is a kind of mutual interference and cannot be seen as separate phenomena.

At the time event of maximum roll angle, and thus of zero global FPSO roll velocity, the fluid velocity at the bilge keel tip is not exactly zero. In fact, very locally, relative high fluid velocities are still seen. In absolute value the velocity (about 0.45 m/s, model scale) is lower than the fluid velocity at the detachment point at even keel (about 0.6 m/s). At maximum roll angle the pressure distribution on the both sides of the appendage is seen to be very similar and symmetrical. This means that the actual drag force on the bilge keel will be small (as expected for this time event in a decay). But, due to the fluid inertia the bilge keel drag is not exactly zero and a small phase shift will exist between the global vessel motions and the bilge keel force. This was actually measured on FPSO-2, and it is a point of further investigations. This insight also reveals that a local bilge keel force model, based on the global roll velocity, cannot accurately model the bilge keel drag force.

The flow visualizations in Figure 17 and 18 also show how the recirculation around the bilge keel is affected by the presence of the hull. The extent of the bilge keel vortex is not only related to the fluid velocities but also influenced by its interaction with the hull. In Figure 18 the fluid field is given at the maximum roll angle with a bilge keel that is slightly higher than the one in Figure 17. In both figures the flow velocity vectors are added which indicate the fluid direction. As can be seen, in both situations there is a significant flow velocity along the keel of the vessel towards the bilge keel. This velocity is partly induced and strengthened by the created vortex from the previous oscillation. The location of the vortex centre is not that different between the two cases, but the intensity and the interaction with the hull differs distinctly due to only the increased bilge keel height.

Another flow visualization example is given in Figure 19. It shows the fluid velocity direction and magnitude around the riser balcony. Due to the fact that the edge of the balcony is relatively far from the hull, the flow interaction with the hull is less compared to the flow interactions near the bilge keel at $t=0$.

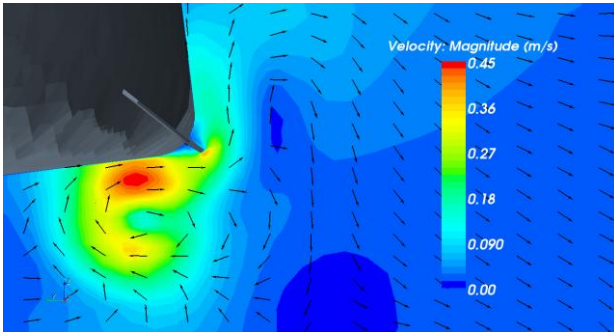


Figure 17: Velocity field around the bilge keel at $t=0$ from the decay with pre-oscillations, bilge keel height 1.2 m

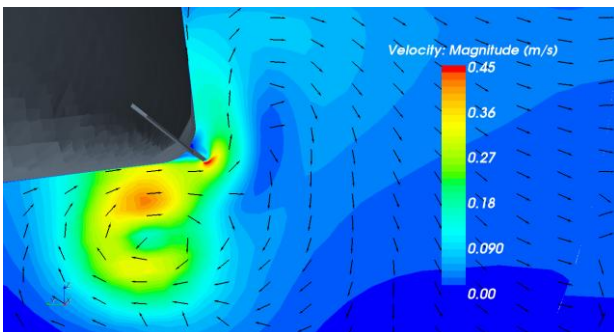


Figure 18: Velocity field around the balcony at $t=0$ from the decay with pre-oscillations, bilge keel height > 1.2 m.

The figures shown give fundamental insight why increasing the appendage height will reduce its damping efficiency when a critical height is reached. It is to a large extent associated with the location of the vortex and its interaction with the hull. Traditionally, the bilge keel damping is considered to vary linearly with its dimensions [6] and this is an important design rule in bilge keel design. It remains valid as long as the created vortex due to flow separation can interact ‘well’ with the hull surface (the pressure interaction in the bilge keel model of Ikeda). The lower efficiency of higher bilge keels agrees with SBM experiences from model tests in several other projects.

The figures demonstrate that the flow physics from a bilge keel and riser balcony are very similar. The dimensions of the vortex, and the fluid velocity in it, from the riser balcony (height 4.7 m) and the bilge keel (height 1.20 m) are very comparable. This might indicate that its extend and physical properties are dominantly driven by the fluid velocities induced by the global roll motion, more than by the local details. Due to the fact that the riser balcony edge is much further away from the hull surface than the bilge keel tip, it makes the bilge keel a more efficient damping device than the riser balcony, which will to less extent influence the hull pressure.

This study shows that the CFD simulation can be used to study flow details around the appendages. The flow details can help to derive a (simplified) model that

characterize the drag on the bilge keels and on the hull due to viscous effect. Efforts will be made in this direction by future investigations. This will enhance the understanding of the relation between roll velocity and the relative flow velocities seen by the bilge keels, as well as a corresponding KC dependent drag value embedding all bilge keel related effects on the roll damping. The expectation is that this can be combined with the local flow velocities induced around the bilge keel for a vessel moving in waves.

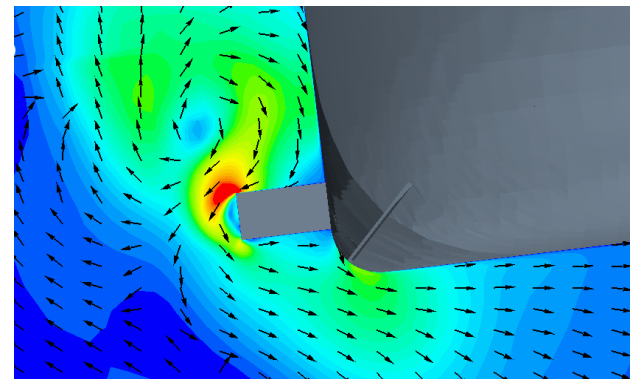


Figure 19: Velocity vector field around the balcony at $t=0$ from the decay with pre-oscillations

7. MOTION PREDICTION IN A SEA STATE

The influence of the quadratic roll damping (B2) coefficient on the motion prediction in pure beam seas is briefly reported. For this purpose the hydrodynamic model of FPSO-1 is used. The added B2 is varied within the (accuracy) range of the decay tests as obtained in model test basin and CFD simulations. The influence of B2 on the standard deviation and thus on the most probable extreme value is given in Figure 20. The two selected sea states have a DEC wave height and a peak period as indicated.

The results show that a certain % variation in B2 results in a much lower % variation in the roll motion prediction. The reduction is about a factor of three in terms of percentage. Still, a variation of this magnitude in the motion prediction can result in a situation that the vessel complies or not to specified criteria.

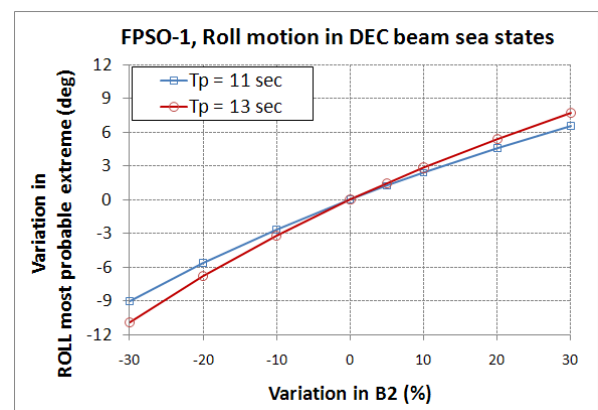


Figure 20: Influence of B2 variation on beam roll motion

8. CONCLUSIONS

Based on the findings presented in this paper it is concluded that the in theory simple and often used free-decay tests can suffer from memory effects. These memory effects are large if the fluid is in rest at the start of the decay, as is the case in a held-over decay test. Significant memory effects will reduce the damping in the first oscillation(s) of the decay, but can increase the damping in the consecutive oscillation(s). So, simply removing the first oscillation period in a free-decay is not always sufficient.

Similar flow memory effects as in model scale experiments are experienced in CFD simulations. Depending on the execution history (either in CFD or in model tests) the quadratic damping coefficient can vary by as much as 25%.

The damping from the riser balcony and bilge keel due to similar flow physics: flow separation from the appendage edge (tip) and dynamic pressure decrease on the leeward appendage side. The drag from the riser balcony is considered to occur from these phenomena and the projected balcony area is a dominant parameter for the damping magnitude. The quadratic damping from the bilge keel is due to the drag on the bilge keel area and to a large extent as well from the pressure change on the hull in the wake of the bilge keel.

The large variation in quadratic damping implies that a prediction in a sea state based on a hydrodynamic model calibrated by a B2 from a decay test has significant uncertainty. It is shown that a variation of about 20% in the quadratic damping leads to about 6% variation in the motion prediction of the most probable extremes. For this reason, the motion predictions in the Petrobras P-57 and Cidade de Paraty FPSO projects were based on a numerical model calibrated with quadratic damping as experienced in design extreme condition sea states. This is considered to be the most realistic approach.

SBM will continue to investigate the physics related to roll damping on offshore structures through CFD and model test analyses. The role of CFD will increase in accumulating knowledge on local flow behaviour, since it is through this that a consistent and realistic roll damping model can be developed. In such a model the KC dependency and the flow memory effects should be addressed. A vision that is already written down 25 years ago by Ikeda [4].

9. ACKNOWLEDGEMENT

The authors wish to thank Petrobras for permitting publication of experimental data obtained from two recent SBM projects, which were carried out for Petrobras.

10. REFERENCES

- [1] WOLFRAM, J., 'On alternative approaches to linearization and Morison's equation for wave forces', *Proc. R. Soc. London*, Vol. 455, pp. 2957-2974, 1988
- [2] VAN 'T VEER, R., 'Application of Linearized Morison Load in Pipe Lay Stinger Design', *27th OMEA Conference*, Portugal, 2008
- [3] Di PAOLA, M. et al, 'Stochastic Seismic Analysis of Structures with Nonlinear Viscous Dampers', *J. of Structural Engineering*, pp. 1475-1478, October 2007
- [4] IKEDA, Y., 'On the Form of Nonlinear Roll Damping of Ships', *A technical note from Institut für Schiffs- und Meerestechnik*, Berlin, ISM-Bericht 83/15, 1983
- [5] CHAKRABARTI, S.K., 'The Theory and Practice of Hydrodynamics and Vibration', *Advanced Series on Ocean Engineering*, Vol. 20, 2002
- [6] HIMENO, Y., 'Prediction of Ship Roll Damping – State of the Art', *Report 239, Dept. of Naval and Marine Eng.*, University of Michigan, 1981
- [7] IKEDA, Y., OSA, K., TANAKA, N., 'Viscous Forces Acting on Irregular Oscillating Circular Cylinders and Flat Plates', *Trans. of the ASME*, No. 140, Vol. 110, 1988
- [8] ROBERTS, J.B., 'Estimation of Nonlinear Ship Roll Damping from Free-Decay Data', *J. of Ships Research*, Vol. 29, No. 2, pp. 127-138, June 1985
- [9] MATHISEN, J.B. and PRICE, W.G., 'Estimation of Ship Roll Damping Coefficients', *Trans. RINA*, Vol. 127, 1985
- [10] MENTER, F., 'Two-equation Eddy Viscosity Turbulence Models for Engineering Applications', *AIAA Journal*, 32, pp. 1299–1310, 1994

11. AUTHORS BIOGRAPHY

Riaan van 't Veer holds the current position of expert engineering in hydrodynamics at SBM GustoMSC in Schiedam, The Netherlands. In this function he is involved in complex hydrodynamic studies for both commercial as research projects. He plays an active role in further developing the hydrodynamic knowledge for SBM as a company. After a Phd from Delft University of Technology in Hydrodynamics, he was for 8 years employed as project manager in the Maritime Research Institute Netherlands (MARIN) before joining SBM.

Fahd Fathi holds the current position of engineer in charge of the development of CFD at SBM GustoMSC in Schiedam, The Netherlands. In this function he is involved in almost all CFD investigations in GustoMSC. He plays an active role in the application of commercial CFD to all kinds of offshore problems, often in collaboration with the other CFD researchers in SBM worldwide as well as academic research centres. He holds an Master's degree in Aerospace Engineering from Ecole Centrale de Paris (France) and a Master of Science in Applied Mathematics from Oxford University (UK).